https://doi.org/10.1016/j.jfluidstructs.2018.09.007

Immersed Boundary-Finite Difference Lattice Boltzmann method through fluid-structure interaction for viscoplastic fluids

GH. R. Kefayati [a,*], H. Tang [b], A. Chan [a]

[a] *School of Engineering and ICT, University of Tasmania, Hobart, Tasmania, Australia*

[b] *Department of Mechanical Engineering, The Hong Kong Polytechnic University, Kowloon, Hong Kong*

Abstract

In this paper, an immersed boundary-finite difference lattice Boltzmann is proposed to simulate fluid-structure interaction of viscoplastic fluids. For simulation of the viscoplastic fluids, the Bingham model without any regularization of the constitutive law was applied. This method is the combination of Finite Difference Lattice Boltzmann for modelling the fluid motion and the effect of the solid structure is studied by the immersed boundary method (IBM). The accuracy of the method for the simulation of viscoplastic fluids has been validated in a lid-driven cavity. In addition, the fluid structure interaction part was validated by a lid-driven cavity with an elastic bottom wall. The fluid-structure interaction in the presence of viscoplastic fluids for rigid and elastic cases have been studied in two different examples. To study the fluid-structure interaction for a rigid body with the viscoplastic fluid, a rosette-shaped in a lid-driven cavity has been studied. In the case of the elastic bodies, the lid-driven cavity filled with viscoplastic fluids by the elastic bottom wall is simulated. In these studies, the yielded/unyielded sections and streamlines have been depicted for high Rayleigh numbers. The effects of the unyielded development on the elastic/deformable parts are presented.

Key words: Viscoplastic fluid, IBM, FDLBM, Lid-driven cavity, Rosette-shaped

* Corresponding author. Dr. Gholamreza Kefayati (GH. R. Kefayati)
Email addresses: gholamrezakefayati@gmail.com, gholamreza.kefayati@utas.edu.au (GH. R. Kefayati), h.tang@polyu.edu.hk (H. Tang), andrew.chan@utas.edu.au (A. Chan).

1 Introduction

Fluid-structure interaction (FSI) problems have received increasing attention in recent years. The deformations of the solid material are in general large and tightly coupled to the flowing fluid. The solid and fluid components are also typically incompressible. This type of system is particularly challenging to simulate because the governing equations are different in the two regions and the interface location must be clarified. They occur in many fields of engineering and applied science. In some FSI problems, fluids have complex rheological, especially viscoplastic manners, e.g. injection molding, food and chemical industries, blood flows, etc. As we know the elastic structure deforms due to fluid action; mainly pressure and viscous stress. So, the alteration of the viscous stress due to the viscoplastic manner makes the problem more complicated and influences the deformations due to FSI. There are many different methods to study FSI and one of the most practical method among them is immersed boundary (IB) method [1]. In this introduction, we explain viscoplastic fluids, the history of viscoplastc fluids in the selected problem (a lid-driven cavity), Immersed boundary (IB) method, and finally the background of the applied Finite Difference Lattice Boltzmann method (FDLBM) are stated.

1.1 Viscoplastic fluids

Viscoplastic fluids form a special sub-class of non-Newtonian fluids in which the flow field is divided into two regions: the first is an unyielded zone where the fluid is at rest or undergoes a rigid motion, and the second where the fluid flows like a viscous liquid. In fact, below a certain stress yield, the medium enjoys rigidity; above this yield the medium behaves like an incompressible viscous fluid. Thus, the location and shape of the yield surface(s), i.e. the interface between these two sets, is also a part of the solution of flow problems of such fluids. Bingham [2] constituted the viscoplastic fluids based on the above description as follows:

$$\begin{cases} \mathbf{A}(\mathbf{u}) = \mathbf{0}, & K(\boldsymbol{\tau}) \leq \tau_y, \\ \boldsymbol{\tau} = \left(\eta + \frac{\tau_y}{K(\mathbf{u})}\right) \mathbf{A}(\mathbf{u}), & K(\boldsymbol{\tau}) > \tau_y, \end{cases} \tag{1.1}$$

where the viscosity η and the yield stress τ_y are constant, and the two invariants $K(\mathbf{u})$ and $K(\boldsymbol{\tau})$ are defined below:

$$2K^2(\mathbf{u}) = \mathbf{A}(\mathbf{u}) : \mathbf{A}(\mathbf{u}), \quad 2K^2(\boldsymbol{\tau}) = \boldsymbol{\tau} : \boldsymbol{\tau}. \tag{1.2}$$

where

$$\mathbf{A}(\mathbf{u}) = \nabla\mathbf{u} + \nabla\mathbf{u}^T. \tag{1.3}$$

1.2 Viscoplastic fluids in a lid-driven cavity

Fluid flow behaviors inside lid driven cavities have been the subject of extensive computational and experimental studies over the past years (Ghia et al. [3], Botella and Peyret [4], Bruneau and Jouron [5], Shahin and Owens [6], Deng et al. [7], Hou et al. [8]). The lid-driven square cavity flow has been used as a benchmark problem for many numerical methods as it covers a wide range of complex hydrodynamics encompassing recirculation, different vortices structures, singularity, instability, and transition.The lid-driven cavity flow is the motion of a fluid inside a rectangular cavity created by a constant translational velocity of one side while the other sides remain at rest. The lid-driven cavity of visco-plastic fluids have been employed to demonstrate the accuracy of different methods and regularizations in order to simulate viscoplastic materials. Sanchez [9] scrutinised a first order operator spilitting method for the solution of the time dependant variational inequality modeling of Bingham fluids in a lid-driven cavity. Dean and Glowinski [10] studied computational methods for numerical simulation of unseteady Bingham viscoplastic fluids in a lid-driven cavity. The operating splitting method was utilised for the time-discritization. Mitsoulis and Zisis [11] studied the benchmark problem of flow in a lid-driven square cavity which was filled with a Bingham fluid. The the Bingham constitutive equation was modified by the Papanastasiou model [12]. The constitutive equation was solved together with the conservation equations using the finite element method (FEM) as the Bingham number varied between Bn = 0 and 1000. It should be noted that just the creeping fluid (Re=0) was conducted in this study. Neofytou [13] investigated non-Newtonian fluids with generalised Newtonian constitutive equations using a numerical scheme based on the finite volume formulation. Among the studied non-Newtonian fluids, the modified and regularized Bingham model based on the Papanastasiou model [12] was analysed in a lid-driven cavity. Vola et al. [14] proposed a numerical method to calculate unsteady flows of Bingham fluids without any regularization of the constitutive law in a lid-driven cavity. The strategy was based on the combination of the characteristic/Galerkin method to cope with convection and of the Fortin–Glowinsky decomposition/coordination method to deal with the non-differentiable and nonlinear terms that derive from the constitutive law. The results were presented for both creeping and non-creeping flows. Huilgol and You [15] studied incompressible and compressible Bingham fluids in a lid-driven cavity, using the exact Bingham model for the constitutive equation as the operator-splitting numerical method was applied to solve the problem. It was indicated that the variational inequalities for incompressible viscoplastic fluids depends

largely on the existence of the viscoplastic constraint tensor. Olshanskii [16] applied semi-staggered finite-difference method to simulate Bingham fluids in a lid-driven cavity using the exact Bingham model. A special stabilization is introduced to be achieved optimal approximation properties of the scheme. Zhang [17] investigated the Augmented Lagrange method for Bingham fluid flows in a lid-driven square cavity. Equal-order piecewise linear finite element spaces were applied for both the velocity and the pressure approximations. A mesh adaptive strategy was also proposed based on the regularity of the numerical solutions. Aposporidis et al. [18] studied and simulated the Bingham fluid flow problem, considering both the exact and a regularized model in a lid-driven cavity. They introduced a new formulation for the regularized Bingham flow equations. In addition, their applied mixed formulation compared to a non-regularized solver based on the Augmented Lagrange method. Santos et al. [19] investigated the effect of inertia and rheology parameters on the flow of viscoplastic fluids inside a lid-driven cavity using a stabilized finite element approximation.The viscoplastic material behavior was simulated by the de Souza Mendes and Dutra model which is called SMD fluid. The SMD model is essentially a regularized viscosity function that involves only rheological properties of the material. The incompressible balance equations were coupled with the non-linear SMD model and were approximated by a multi-field Galerkin least-squares method in terms of extra-stress, pressure and velocity.The numerical simulations were validated through the comparison with literature results, for flows of Bingham fluids. Syrakos et al. [20] studied the creeping square lid-driven cavity flow of a Bingham plastic as the test case and the constitutive equation were regularised by the Papanastasiou model. They utilised the the standard SIMPLE pressure-correction algorithm, which was used to solve the algebraic equation system that is produced by the finite volume discretisation. It was shown that using the SIMPLE algorithm in a multigrid context dramatically improves convergence, although the multigrid convergence rates were much worse than for Newtonian flows. The numerical results were compared with reported results of other methods. However, they noted that the convergence of the method becomes slow at high values of the Bingham number and the regularisation parameter. In addition, with the use of a modified multigrid method, the convergence was accelerated considerably compared to the single-grid SIMPLE method. Syrakos et al. [21] extended their previous work on the creeping flow of a Bingham fluid in a lid-driven cavity, to the study of inertial effects, using a finite volume method and the Papanastasiou regularisation of the Bingham constitutive model. They emphasized that the equations become stiffer and more difficult to solve, while the discontinuity at the yield surfaces causes large truncation errors using the finite volume method (FVM). It was added that by regularising the Bingham constitutive equation, it is easy to extend such a solver to Bingham flows since all that this requires is to modify the viscosity function. In this study, they attempted to investigate the strengths and weaknesses of such a method by applying it to the lid-driven cavity problem for a range of Bingham and

Reynolds numbers (up to 100 and 5000 respectively). By employing techniques such as multigrid, local grid refinement, and an extrapolation procedure, they reduced the effect of the regularisation parameter on the calculation of the yield surfaces. Nevertheless, it was reported that the weakness of FVM becomes more noticeable with the rise of the Bingham number. Muravleva [22] implemented the Uzawa-like algorithm to simulated viscoplastic fluids in a lid-driven cavity as the exact Bingham model was applied in the simulation. In addition, the operator-splitting method was used with employing different time-discretization and space-discretization. The results for the steady-state problem verified as they compared to those in the literature for the shape and location of the yield surface.

1.3 Immersed boundary method (IBM)

Peskin [23] introduced the immersed boundary method (IBM) in 1971 when he studied the flow in heart valves. Peskin and his colleagues applied the IBM for multifaious problems of biological fluid mechanics [24–29]. In IBM, Cartesian Eulerian grid points are employed for the solution of governing equations and Lagrangian points to represent the boundary of immersed objects. The main idea in this method is applying the physical boundary as a deformable elastic fiber with high stiffness. A small deformation or movement of the boundary will yield a force that tends to restore the boundary back to its original shape or position. They applied the immersed boundary method in different problems for Newtonian isothermal fluids flows in the absence of other external forces. In fact, the immersed boundary method is a mixed Eulerian–Lagrangian finite difference method for computing the flow interacting with an immersed boundary. Goldstein et al. [30] used a novel technique related to Peskin's immersed boundary approach to introduce solid surfaces into a simulated flow field. The N-S equations permit the presence of an externally imposed body force that may vary in space and time. Forces were chosen to lie along a desired surface and to have a magnitude and direction opposing the local flow such that the flow was brought to rest on an element of the surface. For unsteady viscous flow the direct calculation of the needed force is facilitated by a feedback scheme in which the velocity was used to iteratively determine the desired value. They utilized the approach to simulate 2D flow around cylinders, 3D turbulent channel flow where one boundary was simulated with a force field, and turbulent channel flow over a riblet-covered surface. Lai and Peskin [31] presented a formally second-order accurate immersed boundary method and tested in this paper. It should be noted the applied force term is a special case of the used force term in the study of Goldstein et al. [30]. They applied the scheme to simulate the flow past a circular cylinder and study the effect of numerical viscosity on the accuracy of the computation by comparing the numerical results with those of a

first-order method. The numerical evidence demonstrated that the presented scheme had less numerical viscosity and was therefore a better choice for the simulation of high Reynolds number flows with immersed boundaries. They applied a Newtonian incompressible fluids flows. Zhu and Peskin [32] reported the computer simulation of a flapping flexible filament in a flowing soap film using the immersed boundary method. They studied filament mass and elasticity, gravity, air resistance, and the two wires that bound the flowing soap film. The incompressible viscous N-S equations, which were used to describe the motion of the soap film and filament, were discretized on a fixed uniform Eulerian lattice while the filament equations were discretized on a moving Lagrangian array of points. The interaction between the filament and the soap film was handled by a smoothed approximation to the Dirac delta function. The delta function approximation was used not only to interpolate the fluid velocity and to apply force to the fluid (as is commonly done in immersed boundary computations), but also to handle the mass of the filament, which was represented in this study as delta function layer of fluid mass density supported along the immersed filament. So, in this study, the Lagrangian elastic force term is the combination of the stretching/compression and the bending forces. Kim and Peskin [32] extended the IBM to cover the case of a massive boundary. They solved the N-S equations with a variable mass density. They proposed a new and simple way to give mass to the elastic boundary and show that the method can be applied to many problems for which the boundary mass is important. They proposed the method with the name of "penalty immersed boundary (pIB) method" to calculate the inertial force and ensure the numerical stability. They introduced two boundaries, one of them is massive boundary having all the mass of the elastic immersed boundary, and the other is a massless boundary. So, they replaced the inertia force with a restoring force in order to make the two boundaries move close together. Zhu et al. [34] applied the IBM for Lattice Boltzmann method (LBM) as an alternative N-S equations solver. They used 3D LBM (D3Q19) within the IBM to simulate a viscous flow past a flexible sheet tethered at its middle line in a 3D channel and determine a drag scaling law for the sheet. The added external force due to IBM in this study was similar to the study of Zhu and Peskin [32], including the stretching/compression and bending terms. Tian et al. [35] introduced a modified penalty approach into the flow-structure interaction solver that combines an immersed boundary method (IBM) and a multi-block LBM to model an incompressible flow and elastic boundaries with finite mass. In this study, the inertial force of the thin solid structure is incorporated by connecting this structure through virtual springs to a ghost structure with the equivalent mass. Actually, the applied force due to immersed boundary is similar to the study of the proposed method (pIB) in the study of Kim and Peskin [32]. To demonstrate the ability of the approach, they studied an elastic filament flapping in the Karman gait and the entrainment regions near a cylinder. Zhu et al. [36] considered a deformable plate interacting with a non-Newtonian fluid flow in three dimensions. A power-law function was used

for the constitutive equation of the non-Newtonian fluid. The lattice Boltzmann equation (the D3Q19 model) was employed for modeling the fluid flow. The immersed boundary (IB) method was utilized for modeling the flexible plate and handling the fluid-plate interaction. They, actually, improved their previous study in Zhu et al. [34] from Newtonian fluid to power-law fluid.

1.4 The numerical method

Lattice Boltzmann method (LBM) has been demonstrated to be a very effective mesoscopic numerical method to model a broad variety of complex fluid flow phenomena. Lattice Boltzmann method (LBM) combined with Finite Difference Method (FDM) has been applied for this problem. It was demonstrated to be a successful mesoscopic method for simulation of Non-Newtonian fluids. Independency of the method to the relaxation time in contrast with common LBM provokes the method to solve different non-Newtonian fluid energy equations successfully as the method protects the positive points of LBM simultaneously. Huilgol and Kefayati [37] explained and derived the two and three dimensional equations of continuum mechanics for this method and demonstrated that the theoretical development can be applied to all fluids, whether they be Newtonian, or power law fluids, or viscoelastic and viscoplastic fluids. Following the previous study, Huilgol and Kefayati [38] derived the two and three dimensional equations of this method for the cartesian, cylindrical and spherical coordinates. Kefayati and Huilgol [39] applied this method to simulate the steady flow in a pipe of square cross-section when the pipe is filled with a Bingham fluid. The problem was solved employing the Bingham model without any regularisation. In the next step, Kefayati and Huilgol [40] utilized the mesoscopic method to conduct a two-dimensional simulation of steady mixed convection in a square enclosure with differentially heated sidewalls when the enclosure is filled with a Bingham fluid. The problem was solved by the Bingham model without any regularisations and also by applying the regularised Papanatasiou model.

1.5 The objectives

The main aim of this study is to introduce an innovative mesoscopic method to simulate fluid-structure interaction for viscoplastc fluids as the yielded/unyielded sections have been displayed and the boundary between the fluid and solid parts are clarified. Based on our best knowledge, this is the first study for fluid-structure interaction in viscoplastic fluids based on immersed boundary method. In fact, this approach covers the both complicated subjects (Fluid-structure interaction and Viscoplastic fluids) simultaneously. To validate the

proposed approach for the problem, we compared the results of fluid-structure interaction and viscoplastic fluids, separately. The applied method, which is based on Lattice Boltzmann Method (LBM), has the advantage of this method compared to macroscopic numerical methods (Finite Volume Method (FVM) and Finite Element Method (FEM)). In this approach, the application of the method in the form of the code and the running time declines considerably. For example, we solved the natural convection of viscoplastic fluids with this method in [40] and the running time just took 11232 seconds where we solved the problem by FEM [46] with the same computer and took 95400 seconds. It demonstrates clearly the advantage of the applied approach for viscoplastic fluids in the case of running time. In addition, the method was, easily; implemented compared to FEM in the case of transferring to the programming codes.

In this study, the Bingham model without any regularization has been studied. A FDLBM, applying IBM have been employed to study the problem numerically. Moreover, it is endeavoured to express the effects of different parameters on the fluid flow as well as yielded/unyielded zones. The obtained results were validated with previous numerical investigations.

2 The mathematical model

2.1 Governing equations

The general macroscopic governing equations based on mass and momentum conservation laws for incompressible flows and conservative materials can be written as:

$$\nabla \cdot \mathbf{u} = 0 \quad , \tag{2.1}$$

$$\rho \mathbf{a} + \nabla p - \nabla \cdot \boldsymbol{\tau} = \mathbf{f}, \quad \mathbf{a} = \frac{\partial \mathbf{u}}{\partial t} + (\mathbf{u} \cdot \nabla)\mathbf{u} \quad , \tag{2.2}$$

$\mathbf{f} = \mathbf{f_e} + \mathbf{f_i}$ is the total force term which is the combination of the external force terms $\mathbf{f_e}$ and the force term due to the IBM $\mathbf{f_i}$. $\boldsymbol{\tau}$ is the extra stress tensor and follows the Bingham model which was mentioned in the Eq.(1.1). Due to the discontinuity in the Bingham model, approximate models such as the Papanastasiou [12], Bercovier and Engelman [41], and the bi-viscosity [42] models are used by researchers and different software packages. However, a constitutive equation for a Bingham fluid fully equivalent to the original form

can be used. This method was proposed and developed by Duvaut and Lions [43] and Glowinski [44] and the constitutive equation takes the form

$$\boldsymbol{\tau} = \eta \mathbf{A}(\mathbf{u}) + \sqrt{2}\ \tau_y\ \boldsymbol{\Lambda}, \quad \mathbf{1} : \boldsymbol{\Lambda} = 0, \tag{2.3}$$

where one may call the second order, symmetric, tensor $\boldsymbol{\Lambda}$ the *viscoplasticity constraint tensor*. Note that the traceless condition $\mathbf{1} : \boldsymbol{\Lambda} = 0$ has been imposed on this tensor so that the stress tensor $\boldsymbol{\tau}$ satisfies the condition tr $\boldsymbol{\tau} = 0$. In order to demarcate the flow field into unyielded/yielded zones, one requires that the tensor $\boldsymbol{\Lambda}$ meet the following conditions:

$$\boldsymbol{\Lambda} : \boldsymbol{\Lambda} = \begin{cases} < 1, & \mathbf{A}(\mathbf{u}) = \mathbf{0}, \\ 1, & \mathbf{A}(\mathbf{u}) \neq \mathbf{0}. \end{cases} \tag{2.4}$$

These conditions satisfy those imposed on the stress tensor, viz., $K(\boldsymbol{\tau}) \leq \tau_y$ when $\mathbf{A}(\mathbf{u}) = \mathbf{0}$, and $\tau_y < K(\boldsymbol{\tau})$ when $\mathbf{A}(\mathbf{u}) \neq \mathbf{0}$. The problem of determining where the flow is rigid and where it is liquid-like has been shifted to finding the tensor $\boldsymbol{\Lambda}$ in the flow field such that is satisfies Eq.(2.4). What has been proposed is important for the following reasons:

(1) The constitutive equations Eqs. (2.3) - (2.4) are defined over the entire flow domain, not just where the fluid has yielded.
(2) One searches for the solution velocity field $\mathbf{u}$ and the viscoplasticity constraint tensor $\boldsymbol{\Lambda}$ to determine the yielded/unyielded regions. There are no singularities because one is not trying to find the location of the yield surface(s) through the limit of $\mathbf{A}(\mathbf{u})/K(\mathbf{u})$ as $\mathbf{A}(\mathbf{u}) \to \mathbf{0}$.
(3) However, the equations of motion now involve two unknown fields: a vector field $\mathbf{u}$, and a symmetric tensor field $\boldsymbol{\Lambda}$. The latter requires that there should exist a connection between the velocity field $\mathbf{u}$ and $\boldsymbol{\Lambda}$. Under Dirichlet boundary conditions, it is possible to prove such a relation. Here, we provide a summary of the results. First, we define a set

$$\mathcal{M} = \left\{ \boldsymbol{\mu} | \boldsymbol{\mu} = \boldsymbol{\mu}^T,\ \boldsymbol{\mu} = (\mu_{ij})_{1 \leq i,j \leq 2} \in (L^2(\Omega))^2, ||\boldsymbol{\mu}|| \leq 1 \text{ a.e. on } \Omega \right\} \tag{2.5}$$

and a projection operator $P_{\mathcal{M}}$ through

$$P_{\mathcal{M}}(\mathbf{q}) = \frac{\mathbf{q}}{\max(1, ||\mathbf{q}||)}, \quad \text{a. e. in } \Omega, \quad \forall \mathbf{q} \in (L^2(\Omega))^2. \tag{2.6}$$

Thus, let $\boldsymbol{\Lambda}^0$ be given, say it is $\mathbf{0}$. If $\boldsymbol{\Lambda}^n$ is known, use the constitutive relation Eq.(2.3) to solve for the velocity field $\mathbf{u}^n$, and find $\boldsymbol{\Lambda}^{n+1}$ through the projection:

$$\boldsymbol{\Lambda}^{n+1} = P_{\mathcal{M}}\left(\boldsymbol{\Lambda}^n + r\tau_y \mathbf{A}(\mathbf{u})^n \right), \tag{2.7}$$

where $r > 0$ is a real number to be specified (It should be noted that the acceptable values of r were reported between $0 < r < \eta/2\tau_y^2$ in Dean et al. [47]

and $0 < r < 2\eta/\tau_y^2$ in Muravleva [22]). Successive iterations are performed till convergence is achieved to the desired level of accuracy. Note that the yield surface is the boundary between $||\mathbf{\Lambda}|| < 1$ and $||\mathbf{\Lambda}|| = 1$. Hence, the solution of the boundary value problem delivers in the limit both the velocity field as well as the shape and location of the yield surface. For more information, see [39,40,45,46].

2.2 The Finite Difference Lattice Boltzmann – Immersed Boundary Method

To have the continuity and momentum equations, a discrete particle distribution function f_α is defined where it should satisfy an evolution equation:

$$\frac{\partial f_\alpha}{\partial t} + \boldsymbol{\xi}_\alpha \cdot \nabla_{\mathbf{x}} f_\alpha - G_\alpha = -\frac{1}{\varepsilon\ \phi}(f_\alpha - f_\alpha^{eq}), \tag{2.8}$$

where ε is a small parameter to be prescribed when numerical simulations are considered. ϕ is the relaxation time. The parameter of G_α is is the term representing the total force effect on the distribution function.

To proceed, one assumes that f_α has the following expansion:

$$f_\alpha = f_\alpha^{eq} + \varepsilon f_\alpha^{(1)} + \varepsilon^2 f_\alpha^{(2)} + O(\varepsilon^3). \tag{2.9}$$

The novelty of the approach by Fu and So [48,49] lies in expanding the equilibrium lattice function f_α^{eq} as a quadratic in the particle velocity $\boldsymbol{\xi}_\alpha$:

$$f_\alpha^{eq} = A_\alpha + \boldsymbol{\xi}_\alpha \cdot \mathbf{B}_\alpha + (\boldsymbol{\xi}_\alpha \otimes \boldsymbol{\xi}_\alpha) : \mathbf{C}_\alpha, \tag{2.10}$$

where $\mathbf{B}_\alpha$ is a vector and $\mathbf{C}_\alpha$ is a 2×2 symmetric matrix. The following relations must hold:

$$\sum_{\alpha=0}^{8} f_\alpha^{eq} = \rho, \tag{2.11}$$

$$\sum_{\alpha=0}^{8} f_\alpha^{eq} \boldsymbol{\xi}_\alpha = \rho \mathbf{u}, \quad \mathbf{u} = u\mathbf{i} + v\mathbf{j}, \tag{2.12}$$

$$\sum_{\alpha=0}^{8} f_\alpha^{eq} \boldsymbol{\xi}_\alpha \otimes \boldsymbol{\xi}_\alpha = \mathbf{M}, \tag{2.13}$$

$$\sum_{\alpha=0}^{8} f_\alpha^{(n)} = 0, \quad n \geq 1, \tag{2.14}$$

$$\sum_{\alpha=0}^{8} f_\alpha^{(n)} \boldsymbol{\xi}_\alpha = 0, \quad n \geq 1. \tag{2.15}$$

where

$$\mathbf{M} = \begin{bmatrix} \rho u^2 + p - \tau_{xx} & \rho uv - \tau_{xy} \\ \rho uv - \tau_{xy} & \rho v^2 + p - \tau_{yy} \end{bmatrix}. \tag{2.16}$$

In the above set, ρ is the density, u and v are the components of the velocity field $\mathbf{u}$ in the x and y directions respectively, $\tau_{xx}, \tau_{xy} = \tau_{yx}, \tau_{yy}$ are the stresses which can be defined through any relevant constitutive relation.

Associated to each node is a lattice velocity vector $\boldsymbol{\xi}_\alpha$. It is defined for D2Q9 as follows:

$$\boldsymbol{\xi}_\alpha = \begin{cases} (0,0), & \alpha = 0, \\ \sigma(\cos\Theta_\alpha, \sin\Theta_\alpha) & \alpha = 1,3,5,7, \\ \sigma\sqrt{2}(\cos\Theta_\alpha, \sin\Theta_\alpha), & \alpha = 2,4,6,8. \end{cases} \tag{2.17}$$

Here, the angles Θ_α are defined through $\Theta_\alpha = (\alpha - 1)\pi/4,\ \alpha = 1, \cdots, 8$. The constant σ has to be chosen with care for it affects numerical stability; its choice depends on the problem. The method for finding the parameter σ which satisfies the Courant-Friedrichs-Lewy (CFL) condition is described in the Appendix.

It was demonstrated that the relation between the above parameters and non-dimensional macroscopic values are as follows [37]

$$A_0 = \rho - \frac{2p}{\sigma^2} - \frac{\rho|\mathbf{u}|^2}{\sigma^2} + \frac{\tau_{xx} + \tau_{yy}}{2}, \quad A_\alpha = 0,\ \alpha = 1,2,\cdots,8. \tag{2.18}$$

$$\mathbf{B}_1 = \frac{\rho\mathbf{u}}{2\sigma^2} = \mathbf{B}_\alpha,\ \alpha = 1,3,5,7; \quad \mathbf{B}_\alpha = \mathbf{0},\ \alpha = 0,2,4,6,8. \tag{2.19}$$

Next, the matrices $\mathbf{C}_\alpha$ are such that $\mathbf{C}_0 = 0;\ \mathbf{C}_1 = \mathbf{C}_\alpha,\ \alpha = 1,3,5,7;\ \mathbf{C}_2 = \mathbf{C}_\alpha,\ \alpha = 2,4,6,8$, where

$$\mathbf{C}_1 = \begin{bmatrix} C_{11} & 0 \\ 0 & C_{22} \end{bmatrix}, \quad C_{11} = \frac{1}{2\sigma^4}\left(p + \rho u^2 - \tau_{xx}\right), \quad C_{22} = \frac{1}{2\sigma^4}\left(p + \rho v^2 - \tau_{yy}\right), \tag{2.20}$$

$$\mathbf{C}_2 = \begin{bmatrix} 0 & C_{12} \\ C_{21} & 0 \end{bmatrix}, \quad C_{12} = C_{21} = \frac{1}{8\sigma^4}\left(\rho uv - \tau_{xy}\right). \tag{2.21}$$

The total force effect on the distribution function G_α can be defined as

$$G_\alpha = 0, \quad \alpha = 0, 2, 4, 6, 8, \tag{2.22a}$$

$$G_\alpha = \frac{1}{2\sigma^2}\mathbf{f}\cdot\boldsymbol{\xi}_\alpha, \quad \alpha = 1, 3, 5, 7 \tag{2.22b}$$

2.3 Computation procedure

The main equations of the discrete particle distribution function Eq.(2.8) is solved by the splitting method of Toro [50]. Hence, the equations can be separated into two parts. The first one is the streaming section which is written as

$$\frac{\partial f_\alpha}{\partial t} + \boldsymbol{\xi}_\alpha \cdot \nabla_{\mathbf{x}} f_\alpha - G_\alpha = 0. \tag{2.23}$$

Eqs.(2.23) has been solved with the method of Lax and Wendroff [51] and the following equations are used.

$$\begin{aligned} f_\alpha^{n+1}(i,j) = f_\alpha^n(i,j) &- \frac{\Delta t}{2\Delta x}\xi_\alpha(i)\left[f_\alpha^n(i+1,j) - f_\alpha^n(i-1,j)\right] \\ &- \frac{\Delta t}{2\Delta y}\xi_\alpha(j)\left[f_\alpha^n(i,j+1) - f_\alpha^n(i,j-1)\right] + \\ &\frac{\Delta t^2}{2\Delta x^2}{\xi_\alpha}^2(i)\left[f_\alpha^n(i+1,j) - 2f_\alpha^n(i,j) + f_\alpha^n(i-1,j)\right] + G_\alpha(i)\Delta t + \\ &\frac{\Delta t^2}{2\Delta y^2}{\xi_\alpha}^2(j)\left[f_\alpha^n(i,j+1) - 2f_\alpha^n(i,j) + f_\alpha^n(i,j-1)\right] + G_\alpha(j)\Delta t\ , \end{aligned} \tag{2.24}$$

In Eqs.(2.24), we have put

$$\xi_\alpha(i) = \boldsymbol{\xi}_\alpha \cdot \mathbf{i}, \quad \xi_\alpha(j) = \boldsymbol{\xi}_\alpha \cdot \mathbf{j}, \quad G_\alpha(i) = \mathbf{G}_\alpha \cdot \mathbf{i}, \quad G_\alpha(j) = \mathbf{G}_\alpha \cdot \mathbf{j}. \tag{2.25}$$

Initial conditions for all macroscopic quantities (u_0, v_0, p_0) including the boundary points are given. The initial values of $f_\alpha^{0,eq}$ including the boundary points are determined. These are used as initial values to start the calculation.
With f_α at time t (including the boundary points) known, intermediate values f_α^I is calculated by solving Eqs.(2.24).
Using these f_α^I, the corresponding macroscopic quantities (u_I, v_I, p_I) for all interior grid points are calculated.
The boundary conditions for the macroscopic level are then set as in the finite

difference method.
Using the macroscopic quantities thus determined over the complete domain including the boundary points and invoking Eqs.(2.10), the corresponding $f_\alpha^{I,eq}$ is obtained, including all of the boundary points.

The second part is the collision section which is as follows:

$$\frac{\partial f_\alpha}{\partial t} = -\frac{1}{\varepsilon\phi}(f_\alpha(\mathbf{x},t) - f_\alpha^{eq}(\mathbf{x},t)), \tag{2.26}$$

Eqs.(2.26) can be solved by using the Euler method and the choice of $\varepsilon\phi$ is taken as the time step (Δt). That is

$$\frac{f_\alpha(\mathbf{x},t+\Delta t) - f_\alpha(\mathbf{x},t)}{\Delta t} = -\frac{1}{\varepsilon\phi}(f_\alpha(\mathbf{x},t) - f_\alpha^{eq}(\mathbf{x},t)), \tag{2.27}$$

from which one obtains

$$f_\alpha(\mathbf{x},t+\Delta t) = f_\alpha^{eq}(\mathbf{x},t), \tag{2.28}$$

Due to Eqs.(2.28), the collision step is completed by setting the new value at time $t+\Delta t$ as $f_\alpha^{I,eq}$. Since each set of macroscopic quantities will map uniquely to an equilibrium distribution function and vice versa, the macroscopic quantities thus obtained are, in fact, the values at time $t+\Delta t$, i.e., $(u,v,p)_{t+\Delta t} = (u_I, v_I, p_I)$.

In the Finite Difference Lattice Boltzmann Method (FDLBM) adopted here, the iteration and recovery of the pressure field is similar to the SIMPLE method of Patankar and Spalding [52,53]. As is well known, the SIMPLE method is a guess-and-correct procedure for the calculation of the pressure field. In each iteration, the velocity field is obtained from the first guessed pressure field. Next, using the corrected velocity field, it is possible to find the corrected pressure and this process continues till a very small or zero mass residual is obtained, since the zero mass residual demonstrates that the divergence of the velocity vector field is zero. In FDLBM, the criteria, which is the mass residual in the SIMPLE method, is the difference between the sum of the distribution functions and the fixed density. Thus, the correction of the pressure field and the subsequent correction of the velocity field continues till a small or zero difference exists between this sum and the density. For an in-depth discussion of these matters, see [49]. So, in this approach, the density is assumed constant ($\rho = 1$) for the case of incompressible fluid and the convergence criteria for different meshes is obtained as follows:

$Error = |\rho - 1| = (\Delta t)^2 = 10^{-8}$

One of the main advantages of the current approach is that boundary conditions can be incorporated in a manner similar to macroscopic methods, in contrast with other methods utilised for solving LBM equations. The latter employ complicated special relationships for the discrete particle distribution function (f_α) for each kind of boundary conditions and problems [54,55]. For example, methods such as on-grid and mid-grid bounce back are used when the velocity is zero on the boundary; when the boundary is in motion, bounce-back is used along with a set of linear equations to determine the boundary values f_α. In the method used here, the boundary condition of f_α can be obtained directly from the macroscopic values on the boundaries due to the relationships of the macroscopic values with f_α. As a result, in this method, boundary conditions, especially the Dirichlet conditions, can be included in various problems similar to macroscopic methods and no special equations for f_α are needed to incorporate the boundary conditions. Therefore, we apply the cited macroscopic values on the boundary conditions in directly.

3 Code validation and grid independence

3.1 Lid-driven cavity of Newtonian fluids

In this section, we first test the accuracy of the lid-driven cavity filled with Newtonian fluid at different Reynolds numbers (Re = 100, 400 and 1000). In the present analysis, we have taken the fluid to be laminar, steady, isothermal, incompressible and two dimensional. The flow domain is given by $\Omega = (0, L) \times (0, L)$, and the boundary $\Gamma = \partial\Omega$.

$$\Gamma_1 = \{\mathbf{x} | \mathbf{x} = \{x, y\}, x = 0 \text{ or } L, 0 \leq y \leq L\} \quad , \tag{3.1a}$$

$$\Gamma_2 = \{\mathbf{x} | \mathbf{x} = \{x, y\}, 0 \leq x \leq L, y = 0\} \quad , \tag{3.1b}$$

$$\Gamma_3 = \{\mathbf{x} | \mathbf{x} = \{x, y\}, 0 \leq x \leq L, y = L\} \quad . \tag{3.1c}$$

The boundary condition for the velocity is straightforward: $\mathbf{u}|_{\Gamma_1} = \mathbf{u}|_{\Gamma_2} = 0$ and $\mathbf{u}|_{\Gamma_3} = u_r \mathbf{i}$. In the case of Newtonian fluid, the second term in Eq.(2.3) is equal to zero, the stress tensor is $\boldsymbol{\tau} = \eta\, \mathbf{A}(\mathbf{u})$. The non-dimensional governing equations based on the above assumptions, boundary conditions and the following non-dimensional variables are as

$$\bar{\mathbf{x}} = \frac{\mathbf{x}}{L}, \quad \bar{\mathbf{u}} = \frac{\mathbf{u}}{u_r}, \quad \bar{p_d} = \frac{p_d}{\rho u_r^2} \quad . \tag{3.2}$$

where u_r is the the speed of the upper wall, p_d is the dynamic pressure. By dropping the bar notation, the following system of non-dimensional mass and momentum equations is derived:

$$\nabla . \mathbf{u} = 0 \quad , \tag{3.3}$$

$$\mathbf{u} \, . \, \nabla \mathbf{u} = -\nabla p_d + \frac{1}{Re} \nabla^2 \mathbf{u} \tag{3.4}$$

The Reynolds number is given by:

$$Re = \frac{L \, \rho \, u_r}{\eta} \quad . \tag{3.5}$$

For solving the problem by FDLBM, in Eqs.(2.20)-(2.21), just we need to replace the stress tensors by $\boldsymbol{\tau} = \frac{1}{Re} \mathbf{A}(\mathbf{u})$, the total force effect on the distribution function in Eq.(2.22) should be equal to zero ($G_\alpha = 0$). The density is selected $\rho = 1$, the top wall velocity is fixed at $u_r = 1$, and the time step is equal to $\Delta t = 0.0001$. An extensive mesh testing procedure has also been conducted to guarantee a grid independent solution. Five different mesh combinations were explored for the case of Re= 1000. It was confirmed that the grid size (200*200) ensures a grid independent solution as portrayed in Table.1. To check the accuracy of the present results, the code was validated with published studies in the literature on the lid-driven cavity flow [3–8]. The results in Table.2 show a good agreement between the compared studies.

3.2 Lid-driven cavity of viscoplastic fluids

In the second validation, the lid-driven cavity filled with Bingham fluid is studied. So, we follow the Eq.(2.3) for the stress tensor and with the cited non-dimensional variables in Eq.(3.2), the studied non-dimensional equations are

$$\mathbf{u} \, . \, \nabla \mathbf{u} = -\nabla p_d + \frac{1}{Re} \nabla . \boldsymbol{\tau}, \tag{3.6}$$

For solving the problem by FDLBM, in Eqs.(2.20)-(2.21), just we need to replace the stress tensors by $\boldsymbol{\tau} = \left[\mathbf{A}(\mathbf{u}) + \sqrt{2} \, Bn \, \boldsymbol{\Lambda} \right]$, the total force effect on the distribution function in Eq.(2.22) should be equal to zero ($G_\alpha = 0$), and $\boldsymbol{\Lambda}$ in Eq. (2.7) changes in this problem to $\boldsymbol{\Lambda}^{n+1} = P_{\mathcal{M}} \left(\boldsymbol{\Lambda}^n + \mathrm{r} \frac{\mathrm{Bn}}{\mathrm{Re}} \mathbf{A}_1^n \right)$. The Bingham

number is $Bn = \frac{\tau_y L}{\eta u_r}$. The density is selected $\rho = 1$, the top wall velocity is fixed at $u_r = 1$, and the time step is equal to $\Delta t = 0.0001$. An extensive mesh testing procedure was conducted to guarantee a grid independent solution. Seven different mesh combinations were explored for the case of Re=1000 and Bn=10. The present code was tested for grid independence by calculating the u and v velocities in the middle of the cavity. It was confirmed that the grid size (250-250) ensures a grid independent solution as portrayed by Table.3 . The accuracy of the applied code in a lid-driven cavity is validated through a comparison with Neofytou [13]. The results are shown in Fig.1 where the u and v velocities profiles demonstrate the accuracy of the present simulation for Bn = 1 and Re = 100. In addition, the yielded/unyielded region and the streamlines are validated by Syrakos et al.[21] at Re=1000 and Bn=10 in Fig.2. The yielded and unyielded parts have been specified by white and black colors in the contour; respectively. It should be mentioned that Neofytou [13] and Syrakos et al.[21] have applied the regularized method of Papanastasiou model in their studies. Results of the FDLBM using the Bingham model is compared with the result of Dean and Glowinski [10]. The streamlines and the yielded/unyielded regions in Fig.3 are depicted at Re = 0.53, Bn = 0.1 which refer to the values of U = 1, μ (η) =1, g (τ_y) = 0.1 in the study of Dean and Glowinski [10] where the values of Reynolds and Bingham numbers found by Huilgol and You [15].

3.3 A bottom elastic wall in a lid-driven cavity

To demonstrate the accuracy of the code for the immersed boundary through fluid-structure interaction, we study the deformation of a soft wall by fluid flow, in a lid-driven cavity flow filled by a Newtonian fluid. The cavity is 2 $\times$ 2, and the deformable bottom volume is initially 2 $\times$ 0.5 occupied by a neo-Hookean wall and the upper part filled with fluid. The lid velocity is

$$u_r = 0.5 \begin{cases} sin^2(\pi x/0.6), & 0 \leq x \leq 0.3, \\ 1 & 0.3 < x < 1.7, \\ sin(\pi(x-2)/0.6), & 1.7 \leq x \leq 2.0. \end{cases} \tag{3.7}$$

The fluid and solid dynamic viscosities are $\eta_f = \eta_s = 0.2$. This case has been studied by many researchers [56–59] with different methods. We applied the Reynolds number of $Re = 5$ as Huang and Sung [57] used this Reynolds number for this case. Here, we utilized the IBM-FDLBM to solve the problem. The basic macroscopic equations and the process is similar to the lid-driven cavity of Newtonian fluid. The only difference is the presence of the force term due to the IBM. For this problem, the force term due to immersed boundary

method is as follows:

$$\mathbf{f_i}(\mathbf{x},t) = \int \mathbf{F}(s,t)\,\delta\left(\mathbf{x}-\mathbf{X}(s,t)\right)ds \tag{3.8}$$

$$\frac{\partial \mathbf{X}(s,t)}{\partial t} = \mathbf{u}(\mathbf{X}(s,t),t) = \int \mathbf{u}(\mathbf{x},t)\,\delta\left(\mathbf{x}-\mathbf{X}(s,t)\right)d\mathbf{x} \tag{3.9}$$

The δ is a two-dimensional Dirac delta function and mentioned [23–29]

$$\delta(\mathbf{x}) = \delta(x)\,\delta(y) \tag{3.10}$$

$$\delta(x) = \begin{cases} \frac{1}{4h}\left(1+cos(\frac{\pi x}{2h})\right), & |x| \le 2h, \\ 0, & |x| \ge 2h, \end{cases} \tag{3.11}$$

where $h = \Delta x = \Delta y$

$$\mathbf{F}(s,t) = \mathbf{F}_s(s,t) + \mathbf{F}_b(s,t) \tag{3.12}$$

The stretching/compression force $\mathbf{F}_s$ at mth node, a finite-difference scheme is used, i.e.,

$$\mathbf{F}_s(s,t) = \frac{\partial}{\partial s}\left[T(s)\frac{\partial \mathbf{X}}{\partial s}\right] \tag{3.13}$$

$T(s)$ is the tension which is computed by Hook's law as follows

$$T(s) = K_s\left(\left|\frac{\partial \mathbf{X}}{\partial s}\right| - 1\right) \tag{3.14}$$

$$\frac{\partial}{\partial s}\left[T(s)\frac{\partial \mathbf{X}}{\partial s}\right]_m = \frac{T_{m+1/2}\,\mathbf{t}_{m+1/2} - T_{m-1/2}\,\mathbf{t}_{m-1/2}}{\Delta s} \tag{3.15}$$

where $\mathbf{t}$ is the unit tangent vector defined at each point and is written

$$\mathbf{t} = \frac{\partial \mathbf{X}}{\partial s} \tag{3.16}$$

The bending force term is $\mathbf{F}_b$ as

$$\mathbf{F}_b(s,t) = K_b \frac{\partial^4 \mathbf{X}}{\partial s^4} \tag{3.17}$$

where

$$\frac{\partial^4 \mathbf{X}}{\partial s^4} = \frac{\mathbf{X}_{m+2} - 4\mathbf{X}_{m+1} + 6\mathbf{X}_m - 4\mathbf{X}_{m-1} + \mathbf{X}_{m-2}}{\Delta s^4} \tag{3.18}$$

In this problem, the stretching and bending coefficients are fixed at $K_s = 0.1$ and $K_b = 0.0001$; respectively. In this study, the selected Eulerian grid is 200 $\times$ 100 in x, y directions where $\Delta x = \Delta y = 1/100$. For the immersed boundary points, we use set of M Lagrangian points which is equal to $M = 100$ and the initial boundary mesh width is $\Delta s = 0.01$. The present results were compared with previous studies in Fig.4 and demonstrates a good agreement.

4 Numerical examples

4.1 Complex rigid body

In the first example, we studied the fluid flow and yielded/unyielded sections around a rigid complex geometry. We simulated a lid-driven cavity filled with viscoplastic fluids in the presence of a rigid rosette-shaped where the lid velocity is equal to $u_r = 1$. The rosette shape of the cylinder is obtained by considering the following relationship between the local radius R_a (distance from the center of the cylinder and a point on the surface) and the angle θ made with the vertical axis [60].

$$R_a(\theta) = R\,(1 + a\,cos8\theta) \tag{4.1}$$

where R is the radius of the reference circular cylinder, and a is a rosette-shape factor. For the rigid body, we applied the method of Lai and Peskin [31] for the force term due to immersed boundary method is as follows:

$$\mathbf{f_i}(\mathbf{x},t) = \int \mathbf{F}(s,t)\,\delta\left(\mathbf{x} - \mathbf{X}(s,t)\right) ds \tag{4.2}$$

$$\frac{\partial \mathbf{X}(s,t)}{\partial t} = \mathbf{u}(\mathbf{X}(s,t),t) = \int \mathbf{u}(\mathbf{x},t)\,\delta\left(\mathbf{x} - \mathbf{X}(s,t)\right) d\mathbf{x} \tag{4.3}$$

$$\mathbf{F}(s,t) = k\left(\mathbf{X}^e(s) - \mathbf{X}(s,t)\right) \tag{4.4}$$

$$\mathbf{X}^e(s) = \mathbf{x_c} + R\left(1 + a\, cos(2\pi * 8\mathbf{x})\right) * cos(2\pi\mathbf{x}) \tag{4.5}$$

where $\mathbf{x_c} = (x_c, y_c)$ is the center of the shape in the cavity. In this problem, we applied the grid 250*250 for the cavity, and the number of points on the immersed boundary is $M = 250$ and the step is $\Delta s = 1/250$. The stiffness was fixed at $k = 1000$ and the applied Dirac delta function is similar to Eqs.(3.10)–(3.11). It should be noted the other applied parameters in FDLBM are the same as the lid-driven cavity filled with the viscoplastic fluid. Fig.5 demonstrates the streamlines, and yielded/unyielded sections for different Bingham numbers at $Re = 200$, $R = 0.1$, $\mathbf{x_c} = 0.5$, and $a = 0.6$. It exhibits that the increase in Bingham number causes the unyielded section to enlarge significantly where the unyielded regions spread to different areas of the cavity. At Bn = 5, the bottom half of the cavity is occupied by the unyielded parts and therefore the horizontal and vertical velocities are zero in the section which results in having no streamlines in this part of the cavity. Fig.6 depicts the streamlines and the yielded/unyielded regions in different parameters in the studied shape at $Re = 200$, and Bn = 1. In the figure (a), we investigated the eccentric shape at $\mathbf{x_c} = 0.7$, $R = 0.1$, and $a = 0.6$. It demonstrates another small vortex in streamlines is generated around the rigid body. Moreover, the shape, size and position of the unyielded sections change considerably. In figure (b), the size of the rigid shape changes as the radius increases by 2 times for the concentric case at $\mathbf{x_c} = 0.5$, $R = 0.2$, and $a = 0.6$. In figure (c), the parameter of a is analysed in the studied shape which changes the sizes of leaves in the Rosette shape at $\mathbf{x_c} = 0.5$, $R = 0.2$, and $a = 0.2$. Fig.7 depicts the streamlines and the yielded/unyielded regions in different Reynolds numbers at Bn = 2, $\mathbf{x_c} = 0.5$, $R = 0.2$, and $a = 0.2$. The streamlines confirms that the rise of Reynolds number results in the movement of the circulation core due to the rise of the forced flow. Moreover, the increase in Reynolds number diminishes the unyielded part in the center of the cavity steadily.

4.2 Deformable bodies

In this part, the studied case of lid-driven cavity with deformable bottom wall; which was employed as a validation, were studied when the Newtonian fluid part was replaced with a viscoplastic fluid. So, the methodology is similar to the Eqs.(3.8)–(3.18). In this simulation, the lid-velocity is fixed $u_r = 1$ and the cavity is 1×1 where the solid part occupies the bottom side from $\mathbf{x} = 0$ to 0.25. In this problem, we applied the grid 250*250 for the cavity, and the number of points on the immersed boundary is $M = 250$ and the step is $\Delta s = 1/250$.

The stretching/compression and bending rigidity coefficients were fixed at $K_s = 0.1$ and $K_b = 0.0001$; respectively. The applied Dirac delta function is similar to Eqs.(3.10)–(3.11). It should be noted the other parts in order to solve by FDLBM is similar to the lid-driven cavity filled with the elastic wall and viscoplastic fluids. Fig.8 demonstrates the streamlines, and yielded/unyielded sections for different Bingham numbers of Bn = 1 and 5 at $Re = 200$. It is clear that the unyielded part is generated the same as a simple lid-drive cavity and just it is generated on the top of the interface position between the viscoplastic fluid and the solid part. Fig.9 shows the streamlines, and yielded/unyielded sections for different Reynolds numbers at Bn = 5. It is clear that the elastic interface becomes more solid as Reynolds number enhances. In addition, the streamline and yielded/unyielded sections demonstrate the same trend as the lid-drive cavity towards the increase in Reynolds number. Fig.10 exhibits the interface position between the solid volume and the viscoplastic fluids for different Bingham and Reynolds numbers. It demonstrates that the rise of Bingham number provokes the alteration of the elastic interface to decline; especially from Bn = 0 to 1, in different Reynolds numbers. Moreover, it reveals that the augmentation of Reynolds number changes the elastic interface position in different Bingham numbers.

5 Conclusion

A numerical approach combining the immersed-boundary method and the Finite Difference lattice Boltzmann method is proposed to simulate the interaction between elastic structures/complex rigid bodies and a viscoplastic fluid flow. The constitutive equation for the Bingham fluid has been applied to the problem without any regularisation. The surface force of the immersed bodies on the fluid is spread into the bulk region as a body force, and the fluid kinematics is simulated by solving the Finite Difference lattice Boltzmann method equation. This proposed method has the ability to be applied for different non-Newtonian fluids for various previous proposed immersed boundary methods whether complicated rigid geometries or deformable sections. However, here, we concentrated on viscoplastic fluids which is more complicated than other forms of non-Newtonian fluids and also for this subclass of non-Newtonian fluids, it is necessary to clarify the yielded/unyielded sections. In addition, the generation of unyielded parts (solid regions) in viscoplastic fluids can affect the deformed parts and this part of this problem can be found by this approach. The studied case is a lid-driven cavity and this approach was validated for Newtonian and viscoplastic fluids by comparison with previous studies. To verify the accuracy of the applied code for the deformable/elastic parts, a lid-driven cavity with a bottom elastic section was studied and showed a good agreement with previous studies. To demonstrate the ability of the proposed

method for the case of a complex rigid body in viscoplastic fluids, we studied a rosette-shaped in a lid-driven cavity for different Reynolds and Bingham numbers. In addition, different positions and forms of the studied rigid body were depicted. Finally, the fluid flow and yielded/unyielded sections were presented in a lid-driven cavity with the bottom elastic section, that the viscoplastic material fills the fluid section. It was demonstrated that the rise of Bingham number declines the change of the elastic interface due to the increase in the unyielded parts. In fact, the enhancement of Bingham number causes the unyielded sections to expand and the fluid flow movement (velocity) to drop considerably. From Eqs.(3.8) to (3.18), the decline of the fluid flow movement (velocity) decreases the deformation due to the bottom elastic wall. Moreover, the increases in Reynolds number (or the forced flow) decreases the movement of the elastic interface.

Appendix

Here, we shall discuss the stability of the numerical scheme. Finding the parameter σ, we multiply f_α^{eq} with $|\boldsymbol{\xi}_\alpha|^2/2$ and take the sum, which leads to

$$\sum_{\alpha=0}^{8} \frac{1}{2} f_\alpha^{eq} |\boldsymbol{\xi}_\alpha|^2 = p + \frac{1}{2}\rho\,|\mathbf{u}|^2 - \frac{\tau_{xx}+\tau_{yy}}{2}. \tag{A1}$$

Next, it is easy to verify that

$$\sum_{\alpha=0}^{8} G_\alpha |\boldsymbol{\xi}_\alpha|^2 = 0. \tag{A2}$$

Hence,

$$\frac{\partial}{\partial t}\left[p + \frac{1}{2}\rho|\mathbf{u}|^2 - \frac{\tau_{xx}+\tau_{yy}}{2}\right] + \frac{\sigma^2}{2}\rho(\nabla\cdot\mathbf{u}) = O\left(\varepsilon\right). \tag{A3}$$

The Courant-Friedrichs-Lewy (CFL) condition states that [61,62]

$$K = \frac{u\Delta t}{\Delta x} + \frac{v\Delta t}{\Delta y} \leq 1. \tag{A4}$$

This can be used in (A3) and we obtain

$$\left[|\mathbf{u}|^2 + \frac{2p - \tau_{xx} - \tau_{yy}}{\rho}\right] + \sigma^2 K = O\left(\varepsilon\right). \tag{A5}$$

Thus, the lattice speed σ must satisfy

$$\sigma = K_c\sqrt{\left|\frac{\tau_{xx}+\tau_{yy}-2p}{\rho} - |\mathbf{u}|^2\right|}\,, \quad K_c = \frac{1}{\sqrt{K}} \geq 1. \tag{A6}$$

Since the pressure p has to be uniquely defined in a Bingham fluid, one requires that $\tau_{xx} + \tau_{yy} = 0$;. Thus, reduces to

$$\sigma = K_c\sqrt{\left|\frac{-2p}{\rho} - |\mathbf{u}|^2\right|}\,, \quad K_c = \frac{1}{\sqrt{K}} \geq 1 \tag{A7}$$

As a result, the value σ is modified and changes in each iteration as defined through (A7).

References

[1] R. Mittal, G. Iaccarino, Immersed boundary method, Annu. Rev. Fluid Mech. 37 (2005) 239–261.

[2] E. C. Bingham, Fluidity and plasticity, McGraw-Hill, New York (1922).

[3] U. Ghia and K. N. Ghia and C. T. Shin, High-Reynolds number solutions for incompressible flow using the Navier-Stokes equations and a multigrid method, J. Comput. Phys., 48 (1982) 387–411.

[4] O. Botella, R. Peyret, Benchmark spectral results on the lid-driven cavity flow, J. Comput. Phys., 27 (1998) 421–433.

[5] C. Bruneau, C. Jouron , An efficient scheme for solving steady incompressible Navier-Stokes equations, J. Comput. Phys., 89 (1990) 389–413.

[6] M. Sahin, G. R. Owens, A novel fully implicit finite volume method applied to the lid-driven cavity problem: High Reynolds number flow calculations, Int. J. Numer. Meth. Fluids , 42 (2003) 57–77.

[7] G. B. Deng, J. Piquet, P. Queutey, M. Visonneau, Incompressible-flow calculations with a consistent physical interpolation finite-volume approach, Computers & Fluids, 23 (1994) 1029–1047.

[8] S. Hou, Q. Zou, S. Chen, G. Doolen, A.C. Cogley , Simulation of cavity flow by the lattice Boltzmann method, J. Comput. Phys., 1118 (1995) 329–347.

[9] F.J. Sanchez, Application of a first-order operator splitting method to Bingham fluid flow simulation, Comput Math Appl 36 (1998) 71–86.

[10] E. J. Dean, R. Glowinski, Operator-splitting methods for the simulation of Bingham visco-plastic flow, Chin Ann Math 23B (2002) 187–204.

[11] E. Mitsoulis, T. Zisis, Flow of Bingham plastics in a lid-driven square cavity, J. Non-Newtonian Fluid Mech. 101 (2001) 173–180.

[12] T.C. Papanastasiou, Flow of materials with yield, J. Rheol. 31 (1987) 385-404.

[13] P. Neofytou, A 3rd order upwind finite volume method for generalised Newtonian fluid flows, Adv Eng Softw 36 (2005) 664–680.

[14] D. Vola, L. Boscardin, J. C. Latch, Laminar unsteady flows of Bingham fluids: a numerical strategy and some benchmark results, J Comput Phys 187 (2003) 441–456.

[15] R. R. Huilgol, Z. You, Prolegomena to variational inequalities and numerical schemes for compressible viscoplastic fluids, J. Non-Newtonian Fluid Mech. 158 (2009) 113–126.

[16] M. A. Olshanskii, Analysis of semi-staggered finite-difference method with application to Bingham flows, Comput. Methods Appl. Mech. Engrg., 198 (2009) 975–985.

[17] Jianying Zhang, An augmented Lagrangian approach to Bingham fluid flows in a lid-driven square cavity with piecewise linear equal-order finite elements, Comput. Methods Appl. Mech. Engrg. 199 (2010) 3051–3057.

[18] A. Aposporidis, E. Haber, M. A. Olshanskii, A. Veneziani, A mixed formulation of the Bingham fluid flow problem: Analysis and numerical solution. Comput. Methods Appl. Mech. Engrg., 200 (2011) 2434–2446.

[19] D. D. Santos, S. Frey, M. F. Naccache, P. R. Souza Mendes, Numerical approximations for flow of viscoplastic fluids in a lid-driven cavity, J Non-Newtonian Fluid Mech 166 (2011) 667–679.

[20] A. Syrakos, G. C. Georgiou, A. N. Alexandrou, Solution of the square lid-driven cavity flow of a Bingham plastic using the finite volume method. J. Non-Newt. Fluid Mech., 195 (2013) 19–31.

[21] A. Syrakos, G. C. Georgiou, A. N. Alexandrou, Performance of the finite volume method in solving regularized Bingham flows: Inertia effects in the lid-driven cavity flow, J Non-Newtonian Fluid Mech 208-209 (2014) 88–107.

[22] L. Muravleva, Uzawa-like methods for numerical modeling of unsteady viscoplastic Bingham medium flows. Appl. Numer. Math., 93 (2015) 140–149.

[23] C. S. Peskin, Flow patterns around heart valves: A numerical method, J. Comput. Phys. 10 (1972) 252–271.

[24] C. S. Peskin, Numerical analysis of blood flow in the heart, J. Comput. Phys. 25 (1977) 220–252.

[25] M.F. McCracken, C.S. Peskin, A vortex method for blood flow through heart valves, J. Comput. Phys. 35 (1980) 183–205.

[26] C.S. Peskin, David M McQueen, Modeling prosthetic heart valves for numerical analysis of blood flow in the heart, J. Comput. Phys. 37 (1980) 113–132.

[27] Charles S Peskin, David M McQueen, A three-dimensional computational method for blood flow in the heart I. Immersed elastic fibers in a viscous incompressible fluid, Journal of Computational Physics, 81 (1989) 372–405.

[28] Charles S Peskin, David M McQueen, A three-dimensional computational method for blood flow in the heart. II. contractile fibers, Journal of Computational Physics, 82 (1989) 289–297.

[29] C. S. Peskin and B. F. Printz, Improved volume conservation in the computation of flows with immersed elastic boundaries, J. Comput. Phys. 105 (1993) 33–46.

[30] D. Goldstein, R. Handler, L. Sirovich, Modeling a No-Slip Flow Boundary with an External Force Field, J. Comput. Phys. 105 (1993) 345–366.

[31] Ming-Chih Lai, Charles S. Peskin, An Immersed Boundary Method with Formal Second-Order Accuracy and Reduced Numerical Viscosity, Journal of Computational Physics 160, 705–719 (2000).

[32] Luoding Zhu, Charles S. Peskin, Simulation of a Flapping Flexible Filament in a Flowing Soap Film by the Immersed Boundary Method, Journal of Computational Physics 179, 452–468 (2002).

[33] Yongsam Kim, Charles S. Peskin, Penalty immersed boundary method for an elastic boundary with mass, Physics of Fluids 19, 053103 (2007).

[34] Luoding Zhu, Guowei He, Shizhao Wang, Laura Miller, Xing Zhang, Qian You, Shiaofen Fang, An immersed boundary method based on the lattice Boltzmann approach in three dimensions, with application, Computers and Mathematics with Applications 61 (2011) 3506–3518.

[35] Fang-Bao Tian, Haoxiang Luo, Luoding Zhu, James C. Liao, Xi-Yun Lu, An efficient immersed boundary-lattice Boltzmann method for the hydrodynamic interaction of elastic filaments, Journal of Computational Physics 230, 7266–7283 (2011).

[36] Luoding Zhu, Xijun Yu, Nansheng Liu, Yongguang Cheng, Xiyun Lu, A deformable plate interacting with a non-Newtonian fluid in three dimensions, Physics of Fluids 29 (2017) 083101.

[37] R.R. Huilgol, GH.R. Kefayati, From mesoscopic models to continuum mechanics: Newtonian and non-newtonian fluids, Journal of Non-Newtonian Fluid Mechanics 233 (2016) 146-154.

[38] R.R. Huilgol, GH.R. Kefayati, A particle distribution function approach to the equations of continuum mechanics in Cartesian, cylindrical and spherical coordinates: Newtonian and non-Newtonian fluids, Journal of Non-Newtonian Fluid Mechanics 251 (2018) 146–154.

[39] GH. R. Kefayati, R.R. Huilgol, Lattice Boltzmann method for the simulation of the steady flow of a Bingham fluid in a pipe of square cross-section, European Journal of Mechanics BFluids 65 (2017) 412-422.

[40] GH. R. Kefayati, R.R. Huilgol, Lattice Boltzmann Method for simulation of mixed convection of a Bingham fluid in a lid-driven cavity, International Journal of Heat and Mass Transfer 103 (2016) 725-743.

[41] M. Bercovier, M. Engelman, A finite-element method for incompressible non-Newtonian flows, J. Comput. Phys., 36 (1980) 313-326.

[42] E.J. O'Donovan, R.I. Tanner, Numerical study of the Bingham squeeze film problem, J. Non-Newt. Fluid Mech. 15 (1984) 75-83.

[43] G. Duvaut, J.L. Lions, Transfert de chaleur dans un fluide de Bingham dont la viscosité dépend de la température, J. Funct. Anal. 11 (1972) 93-110.

[44] R. Glowinski, Finite element methods for incompressible viscous flow, Handbook of Numerical Analysis, vol. 9, 2003, 3–1176.

[45] R.R. Huilgol, Fluid Mechanics of Viscoplasticity, Springer, Berlin Heidelberg, 2015.

[46] R.R. Huilgol, GH. R. Kefayati, Natural convection problem in a Bingham fluid using the operator-splitting method, Journal of Non-Newtonian Fluid Mechanics 220 (2015) 22–32.

[47] E. J. Dean, R. Glowinski, G. Guidoboni, On the numerical simulation of Bingham visco-plastic flow: Old and new results, J. Non-Newt. Fluid Mech., 142 (2007) 36–62.

[48] S.C. Fu , R.M.C. So , R.M.C. Leung , Stochastic finite difference lattice Boltzmann method for steady incompressible viscous flows, Journal of Computational Physics 229 (2010) 6084–6103 .

[49] S.C. Fu , R.M.C. So , R.M.C. Leung , Linearized-Boltzmann-type-equation-based finite difference method for thermal incompressible flow, Comput. Fluids 6 (2012) 67–80 .

[50] E.F. Toro , Riemann Solvers and Numerical Methods for Fluid Dynamics: A Prac- tical Introduction, 2nd, Springer-Verlag, New York, 1999.

[51] P.D. Lax, B. Wendroff, Systems of conservation laws, Communication in Pure and Applied Mathematics 13 (1960) 217–237.

[52] S. V. Patankar, D. B. Spalding, A calculation procedure for heat, mass and momentum transfer in three-dimensional parabolic flows, Int. J. Heat Mass Transfer 15 (1972) 1787–1806.

[53] S. V. Patankar, A calculation procedure for two-dimensional elliptic situations, Numerical Heat Transfer 4 (1981) 409–425.

[54] Q. Zou, X. He, On pressure and velocity boundary conditions for the lattice Boltzmann BGK model. Phys. Fluids, 9 (1997) 1591–1598.

[55] Z. Guo, B. Shi, C. Zheng, A coupled lattice BGK model for the Boussinesq equations, Int. J. Numer. Methods Fluids, 39 (2002) 325–342.

[56] Hong Zhao a, Jonathan B. Freund, Robert D. Moser, A fixed-mesh method for incompressible flow–structure systems with finite solid deformations, Journal of Computational Physics 227 (2008) 3114–3140.

[57] Wei-Xi Huang, Hyung Jin Sung, An immersed boundary method for fluid–flexible structure interaction, Comput. Methods Appl. Mech. Engrg. 198 (2009) 2650 – 2661.

[58] Zhi-Qian Zhang, G. R. Liu, Boo Cheong Khoo, Immersed smoothed finite element method for two dimensional fluid–structure interaction problems, Int. J. Numer. Meth. Engng 2012; 90:1292–1320.

[59] Xingshi Wang, Lucy T. Zhang, Interpolation functions in the immersed boundary and finite element methods, Comput Mech (2010) 45:321–334.

[60] F. Ilinca, J.-F. Hetu, Immersed boundar solution of natural convection in a square cavity with an enclosed rosette-shaped hot cylinder, Numerical Heat Transfer, Part A, 65 (2014) 1154–1175.

[61] J. Blazek, (2001) Computational Fluid Dynamics: Principles and Applications. Elsevier, 347–350.

[62] T. Cebeci, J. P. Shao, F. Kafyeke, E. Laurendeau, (2005) Computational Fluid Dynamics for Engineers. Springer, 311–320.

Table 1
Minimum values of u (u_{min}) computed along $x = 0.5$, maximum values of v (v_{max}) computed along $y = 0.5$, minimum values of v (v_{min}) computed along $y = 0.5$ at Re=1000

Mesh	u_{min}	v_{min}	v_{max}
100*100	-0.3501	-0.5109	0.3448
150*150	-0.3722	-0.5193	0.3605
200*200	-0.3840	-0.5279	0.3765
250*250	-0.3840	-0.5279	0.3765
300*300	-0.3840	-0.5279	0.3765

Table 2
(a) minimum values of u computed along $x = 0.5$ and the corresponding ordinate y_{min}, (b) maximum values of v computed along $y = 0.5$ and the corresponding abscissa x_{max}, (c) minimum values of v computed along $y = 0.5$ and the corresponding abscissa x_{min}, (d) minimum values of stream function and the corresponding coordinates x_{min}; y_{min}.

Reference	u_{min}	y_{min}	v_{max}	x_{max}	v_{min}	x_{min}	ψ_{min}
Re=100							
Present	-0.2111	0.4591	0.1802	0.2358	-0.2571	0.8121	-0.1031
Ghia et al. [3]	-0.2109	0.4598	0.1809	0.2354	-0.2566	0.8127	-0.1035
Botella and Peyret [4]	-0.2140	0.4581	0.1796	0.2370	-0.2538	0.8104	-
Bruneau and Jouron [5]	-0.2106	0.4531	0.1786	0.2344	-0.2521	0.8125	-0.1026
Deng et al. [7]	-0.2131	-80.1789	-	-0.2354	-	-	-
Sahin and Owens [6]	-0.2139	0.4598	0.1808	0.2354	-0.2566	0.8127	-0.1035
Hou et al. [8]	-	-	-	-	-	-	-0.1030
Re=400							
Present	-0.3296	0.2882	0.3083	0.2291	-0.4601	0.8911	-0.1162
Ghia et al. [3]	-0.3273	0.2813	0.3020	0.2266	-0.4499	0.8594	-0.1139
Hou et al. [8]	-	-	-	-	-	-	-0.1121
Deng et al. [7]	-0.3275	-	0.3027	-	-0.4527	-	-
Sahin and Owens [6]	-0.3283	0.2815	0.3044	0.2253	-0.4563	0.8621	-0.1139
Re=1000							
Present	-0.3840	0.1721	0.3765	0.1586	-0.5279	0.9105	-0.1184
Sahin and Owens [6]	-0.38810	0.1727	0.3769	0.1573	-0.5285	0.9087	-0.1188
Ghia et al. [3]	-0.3829	0.1719	0.3709	0.1563	-0.5155	0.9063	-0.1179
Botella and Peyret [4]	-0.3886	0.1717	0.3769	0.1578	-0.5271	0.9092	-0.1189
Hou et al. [8]	-	-	-	-	-	-	-0.1178
Bruneau and Jouron [5]	-0.3764	0.1602	0.3665	0.1523	-0.5208	0.9102	-0.1163
Deng et al. [7]	-0.38511	-	0.3769	-	-0.5228	-	-

Table 3
Minimum values of u (u_{min}) computed along $x = 0.5$, maximum values of v (v_{max}) computed along $y = 0.5$, minimum values of v (v_{min}) computed along $y = 0.5$ at Re=1000 and Bn=10

Mesh	u_{min}	v_{min}	v_{max}
150*150	-0.0798	-0.4191	0.2483
180*180	-0.0809	-0.4220	0.2517
200*200	-0.0815	-0.4295	0.2606
220*220	-0.0819	-0.4311	0.2695
250*250	-0.0824	-0.4320	0.2711
280*280	-0.0824	-0.4320	0.2711
300*300	-0.0824	-0.4320	0.2711

List of Figures

numbers

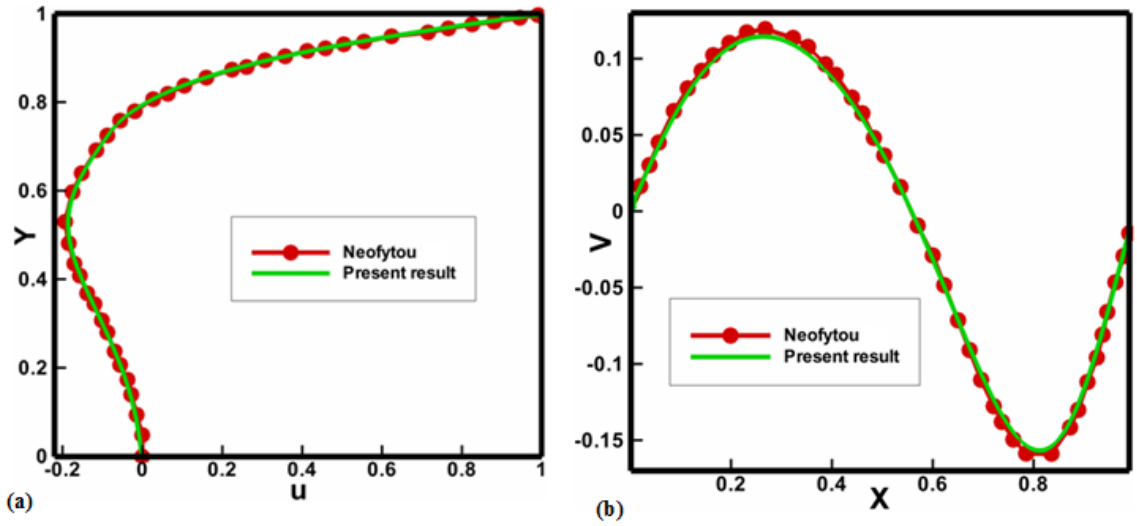

Fig. 1. Comparison of u and v velocities profiles in the middle of the cavity between the present results with the results of Neofytou [13] for Re = 100 and Bn = 1

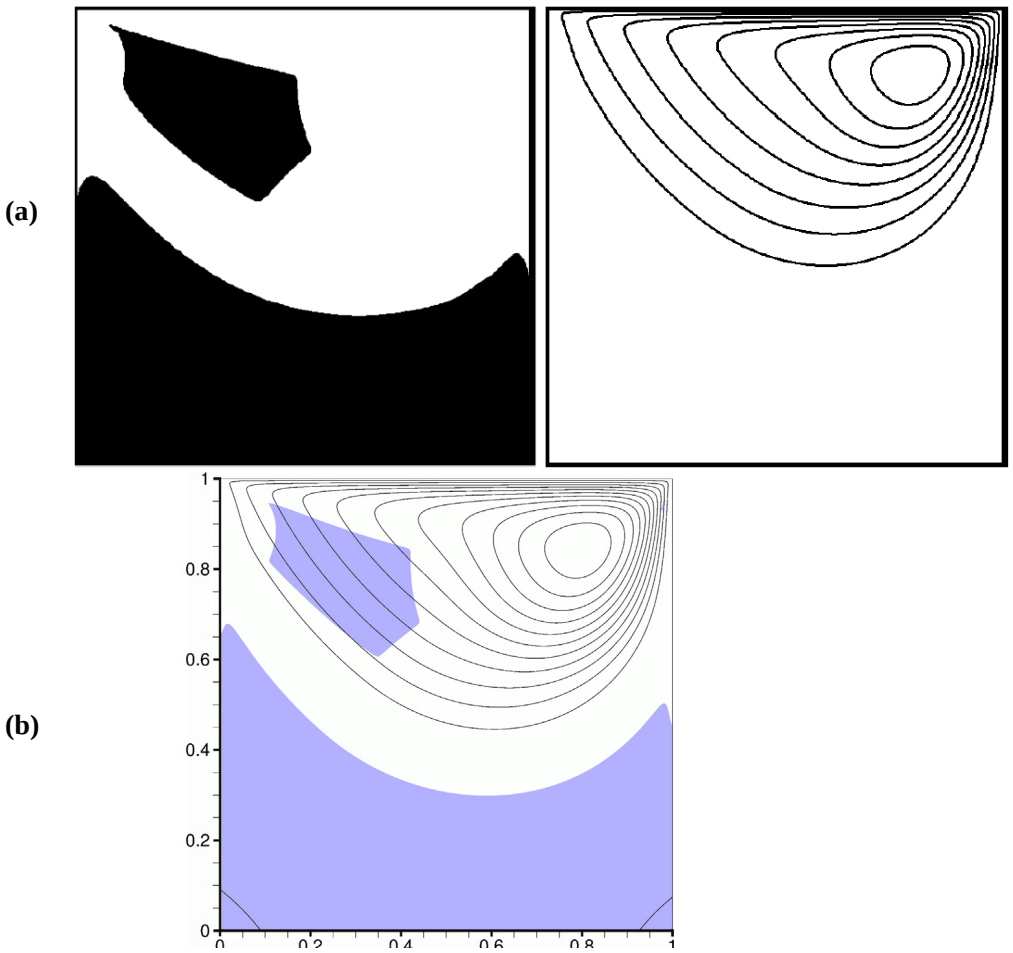

Fig. 2. Comparisons of the streamlines and the yielded/unyielded regions between (a) the present study with (b) the results of Syrakos et al. [21] for Re = 1000 and Bn = 10

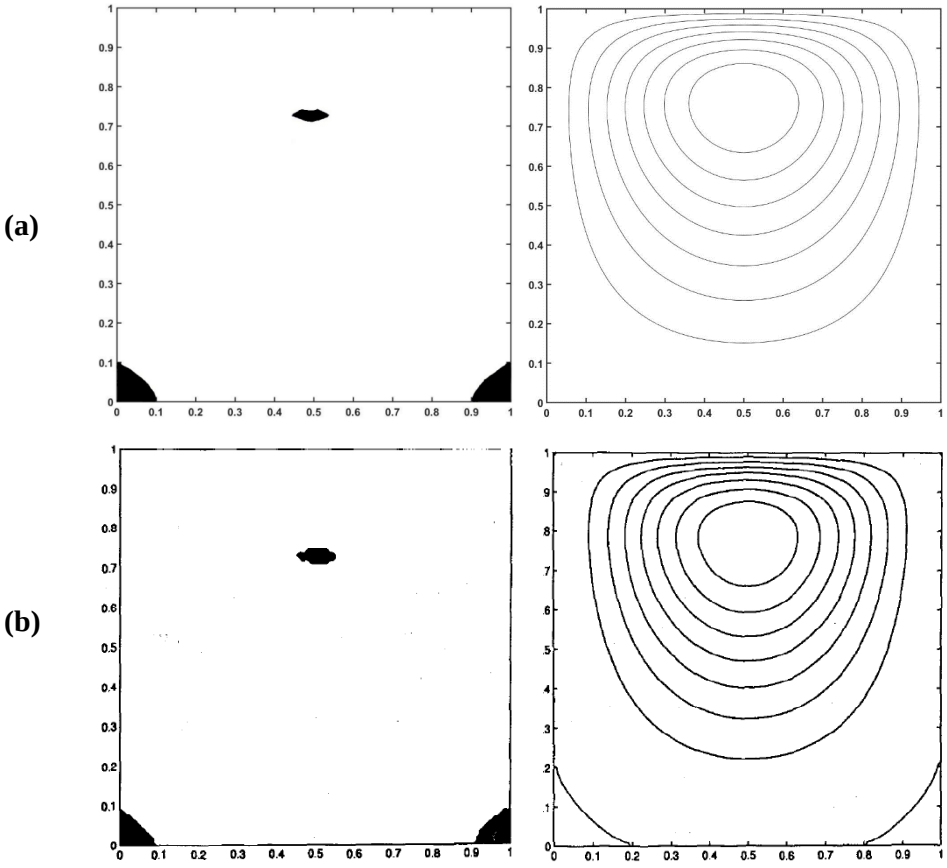

Fig. 3. Comparisons of the yielded/unyielded regions and streamlines between (a) the present study with the results of (b) Dean and Glowinski [10] for Re = 0.53, Bn = 0.1 corresponding to $U = 1$, $\mu = 1$, $g = 0.1$ in Dean and Glowinski [10]

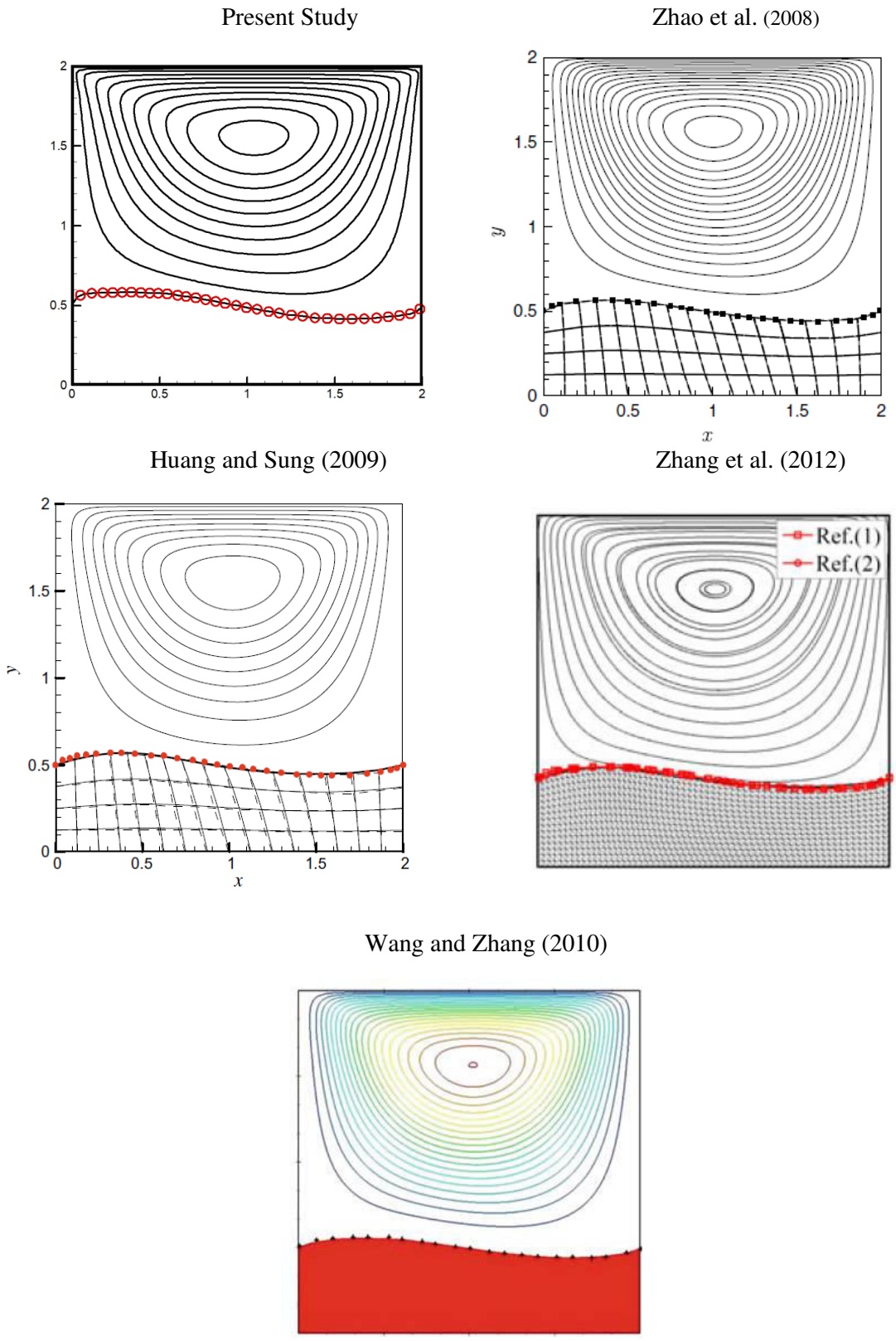

Fig. 4. Comparisons of the streamlines and the interface position between the present study with previous results Zhao et al. [56], Huang and Sung [57], Zhang et al. [58], Wang and Zhang [59]

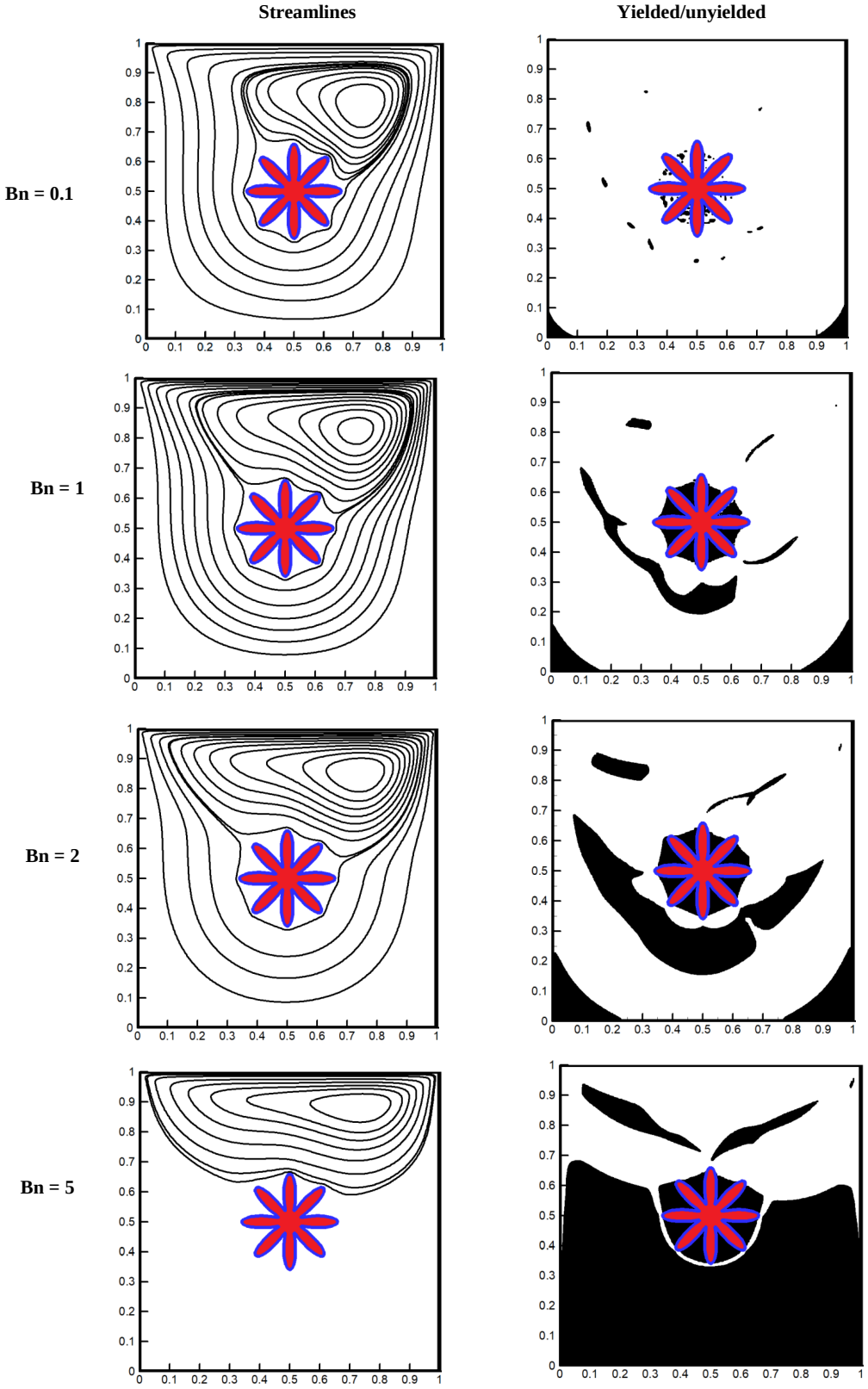

Fig. 5. Comparisons of the streamlines and the yielded/unyielded regions in different Bingham numbers at $Re = 200$, $R = 0.1$, $\mathbf{x_c} = 0.5$, and $a = 0.6$

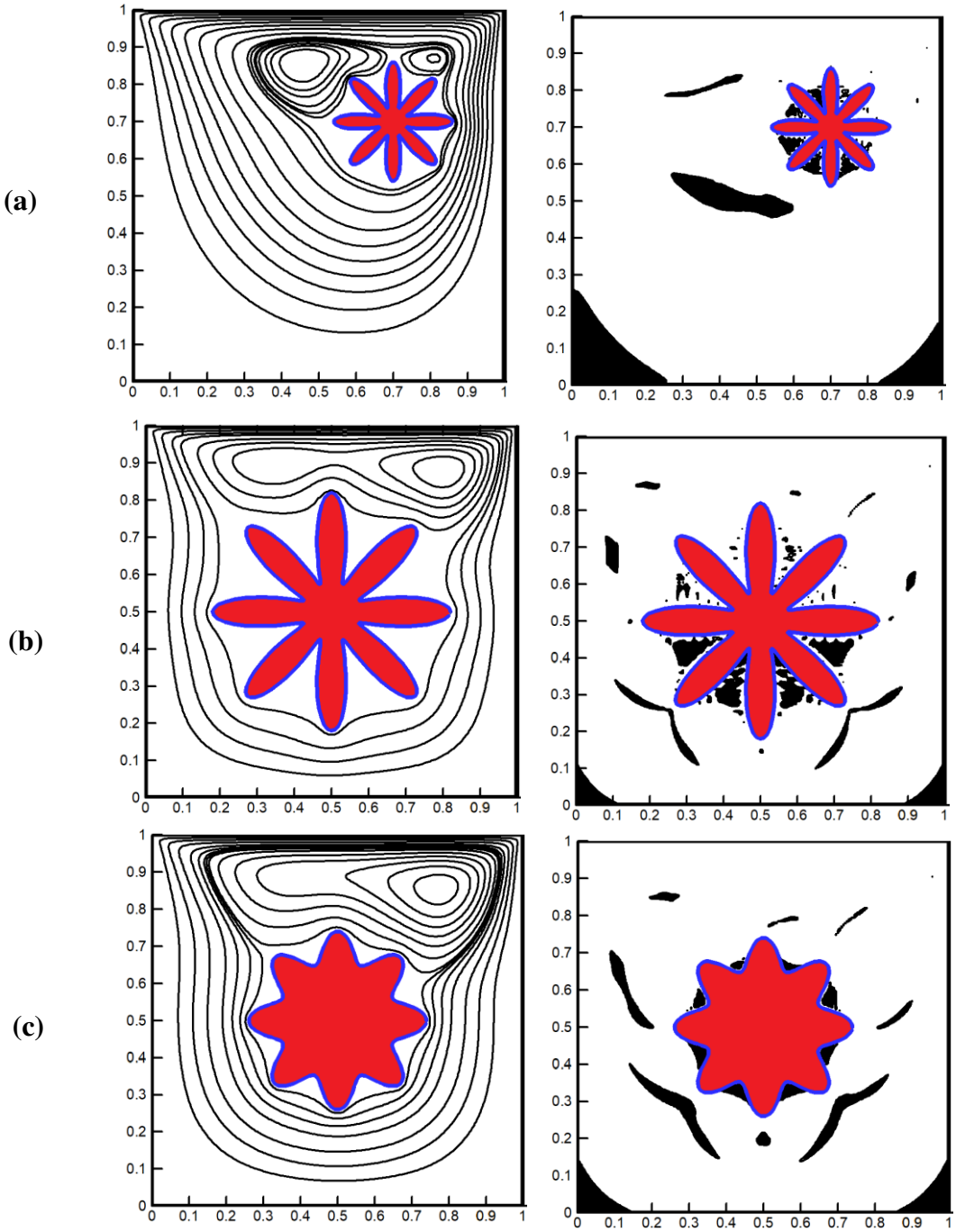

Fig. 6. Comparisons of the streamlines and the yielded/unyielded regions in different parameters in the studied shape at $Re = 200$, and Bn $= 1$ (a) $\mathbf{x_c} = 0.7$, $R = 0.1$, and $a = 0.6$, (b) $\mathbf{x_c} = 0.5$, $R = 0.2$, and $a = 0.6$ (c) $\mathbf{x_c} = 0.5$, $R = 0.2$, and $a = 0.2$

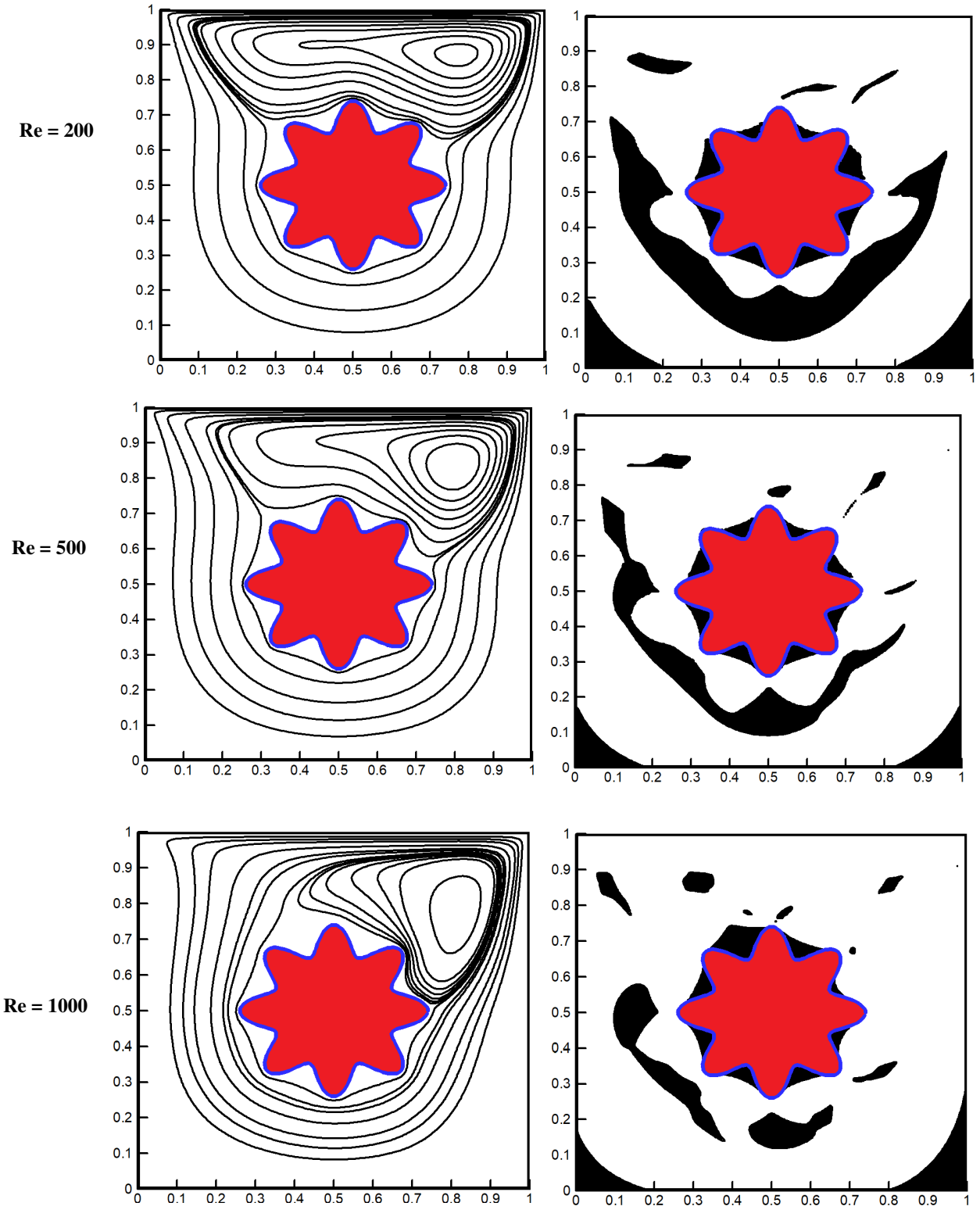

Fig. 7. Comparisons of the streamlines and the yielded/unyielded regions in different Reynolds numbers at Bn = 2, $\mathbf{x_c} = 0.5$, $R = 0.2$, and $a = 0.2$

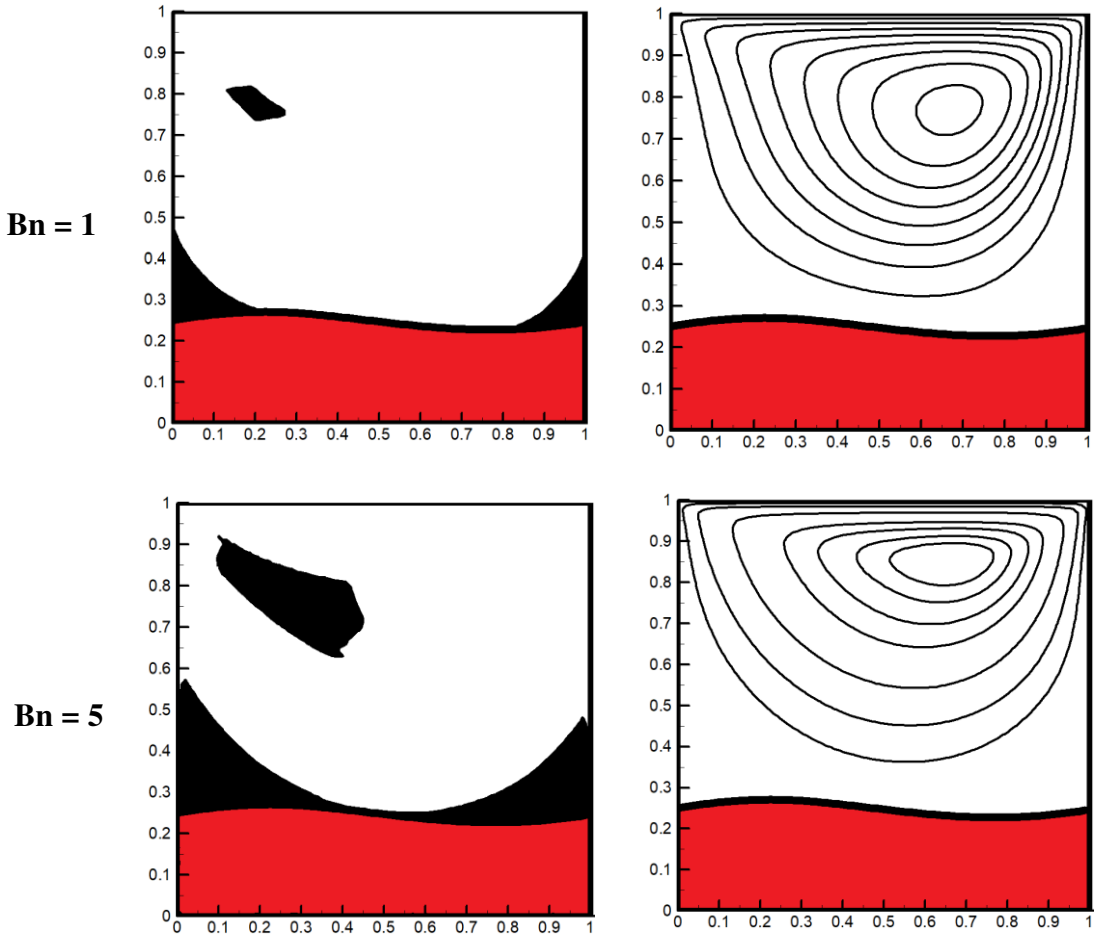

Fig. 8. Comparisons of the streamlines and the yielded/unyielded regions in different Bingham numbers at Re = 200

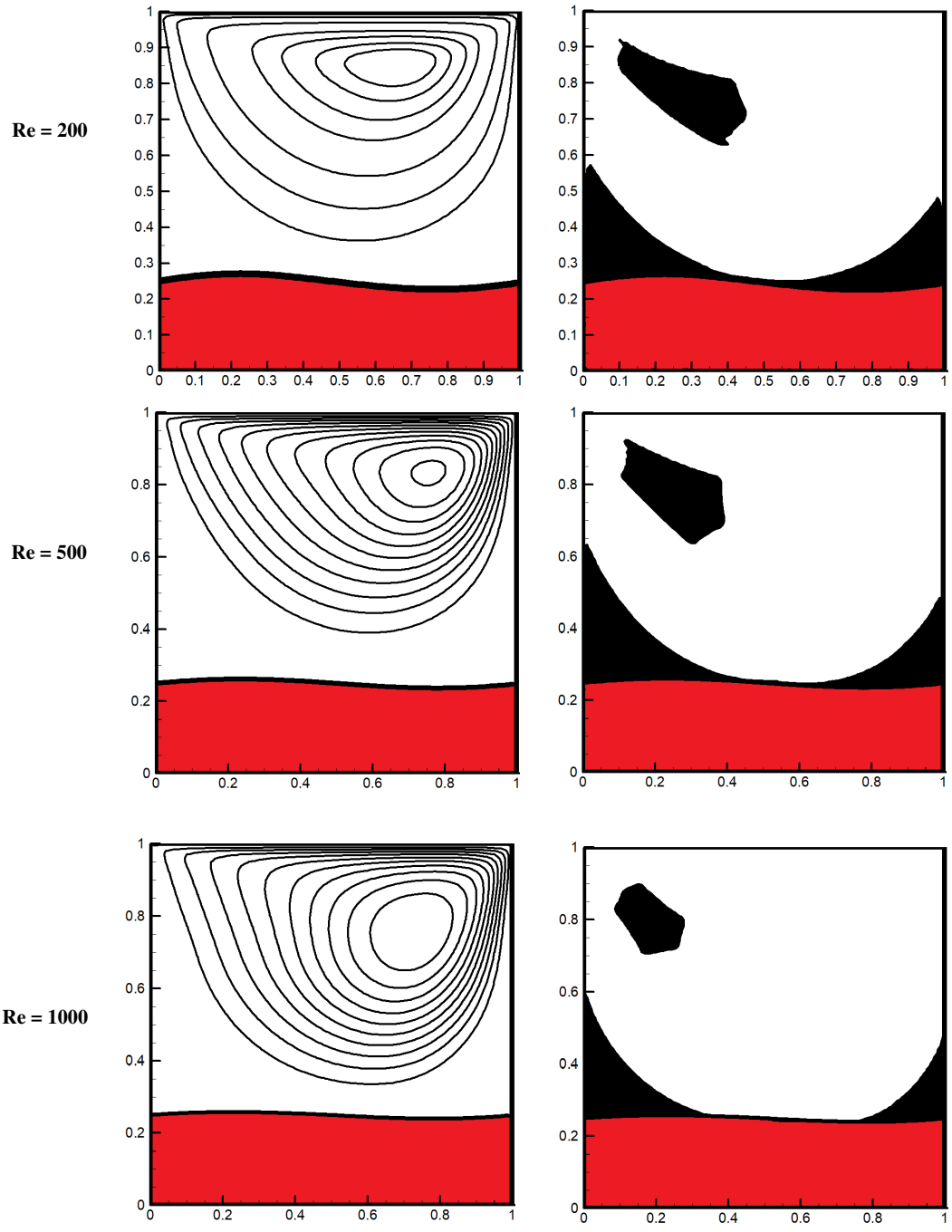

Fig. 9. Comparisons of the streamlines and the yielded/unyielded regions in different Reynolds numbers at Bn = 5

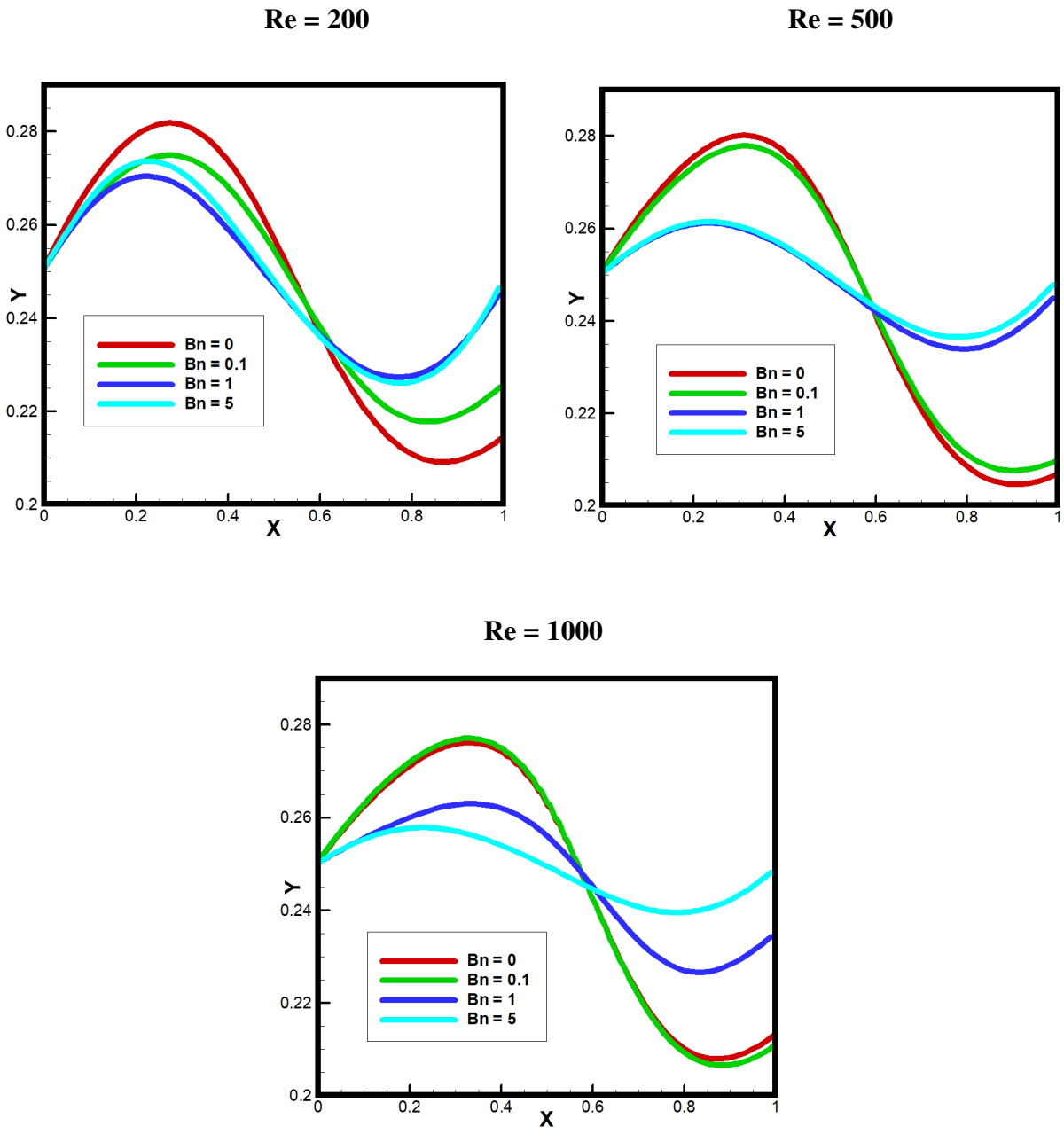

Fig. 10. Comparisons of the interface position in different Bingham and Reynolds numbers